Int. J. Adv. Appl. Math. and Mech. 10(1) (2022) 15 – 27 (ISSN: 2347-2529)

Journal homepage: www.ijaamm.com

IJAAMM

International Journal of Advances in Applied Mathematics and Mechanics

Turbulent Mixed Convection of Heat in a Greenhouse

Research Article

James Kigo*, **Mathew Kinyanjui**, **Roy Kiogora**

Department of Pure and Applied Mathematics, Jomo Kenyatta University of Agriculture and Technology, Juja, 62000-00200, Nairobi, Kenya

Received 08 August 2022; accepted (in revised version) 01 September 2022

Abstract: In this paper a turbulent mixed convection of heat in greenhouse has been investigated. This study considers a greenhouse containing crops with an exhaust fan on the right wall and a window on the left wall.The window acts as the inlet while the fan as the outlet. The flow is transient with variable viscosity and thermal conductivity and the effects of the crops (drag force and sensible heat released during transpiration) are considered. The partial differential equations governing the flow are transformed into non dimensional form and solved by the finite volume method. MATLAB code is employed in solving the discretized partial differential equations. The results for velocity and temperature are presented graphically for various parametric conditions. It is established that the Reynolds number, Richardson number, Prandtl number and aspect ratio either increase,decrease or have no effect on the velocity and temperature profiles. This study provides useful information to greenhouse designers and operators for controlling greenhouse microclimate.

MSC: 76DXX • 76FXX

Keywords: Greenhouse • Mixed Convection • Variable viscosity

1. Introduction

A greenhouse is a closed environment covered with a transparent or translucent material, inside which temperature increases due to the cover holding radiation and also reducing airflow into the structure. The greenhouse cover may be made of glass, flexible plastic films such as polyethylene, polyester, polyvinyl chloride, fibre glass-reinforced plastic, acrylic and polycarbonate rigid panels. The greenhouse protects the crops from rain, heat, cold, and also numerous environmental factors that can slow down or prevent the crops from being grown at any particular time of the year. A desired microclimate is provided and also must accommodate the production system, promote good labour working conditions and minimize external disturbances [1]. Greenhouse microclimate and air components are affected by the air and energy exchange between the exterior and interior. Due to this exchange, the concentration of water vapour and carbon dioxide are affected [2]. In a greenhouse, ventilation helps to control the microclimate which results from complex interactions between the crops, greenhouse structure and external conditions[3]. Due to the greenhouse cover, reduction in mixing of air results in modifications in the convective and radiant exchanges, and this leads to increase in day time temperatures and lesser decreases during night time than outdoors [1].
Generally, greenhouse temperatures are higher than ambient temperatures. These high temperatures increase vapour pressure deficits, leading to an increase in evaporating power of air. The study on greenhouses has been carried out by various researchers. [4] carried out a simulation on the microclimate of a naturally ventilated greenhouse using the

* Corresponding author.
E-mail address(es): kigojamesm@gmail.com (James Kigo).

Gembloux Greenhouse Dynamic Model (GGDM). They introduced the stomatal resistance of vegetation and also improved calculations of a natural ventilation flux. The analysis showed that external wind speed and the opening angle of the vents significantly influenced the ventilation flux. [5] studied the effect of wind direction on climatic parameters inside a greenhouse. A naturally ventilated tunnel-type greenhouse was considered. The geometry of the greenhouse had five vents on each side and five rows of mature tomato crops. The simulations were done with the use of three different models i.e. the renormalisation group (RNG), realizable $k \sim \epsilon$ model and the standard $k \sim \epsilon$ model. The study concluded that the wind direction influenced the temperature, velocity, and humidity distributions. The velocity field computed using the three different models showed noticeable difference in the temperature, velocity and humidity patterns in the greenhouse. This confirmed the importance of choice of the turbulence model.
[6] investigated natural ventilation in a semi- arid greenhouse. Two single-span double-polyethylene greenhouses with high pressure fog nozzles, roll-up side vents with insect screens and roof vent were constructed. They were plant free and the floor was dry filled with gravel and evaporation from the floor was considered to be negligible. The greenhouse and outside conditions were monitored under several configurations. The tracer gas method was used to measure the natural ventilation rate continuously and the fog generated was also collected and measured. It was observed that the relative humidity decreased with an increase in ventilation rate, and the water used for cooling increased. The results showed that the humidity decreased from 80 to 60% approximately on a clear day when ventilation rate was increased from 1 to $3.5 m^3 m^{-2} min^{-1}$. Also, the water used increased from 18 to $21 g m^{-2} min^{-1}$.The control algorithm demonstrated the possibility of maintaining the relative humidity and temperature simultaneously within a desirable range while reducing water used in fog cooling. [7] simulated the climate in two greenhouses with different geometries. The effect of the wind speed were studied and compared between a multi-span greenhouse and a shark-fin shaped greenhouse by two-dimensional CFD. The top and the sides of both geometries were equipped with roll up windows. The areas considered were 24% and 10% of the ground area for the side and roof ventilation respectively in a multi-span greenhouse while for the shark-fin shaped were 28% and 30%. A comparison of the numerical results with experimental data were made. It was observed that the air renewal rate was $27 h^{-1}$ for the multi-span and $75 h^{-1}$ for the shark-fin greenhouse at a wind speed of $4 m s^{-1}$ with fully open windows. Also, the temperature profiles were more homogeneous inside the shark-fin greenhouse than in the multi-span greenhouse.
[8] investigated a greenhouse ventilation efficiency based on a two-dimensional CFD. The effect of roof vent and the wind on air flow and temperature distributions in a compartmentalised glasshouse was analysed numerically. The numerical model was used to study the effect of three different openings on the natural ventilation with only leeward roof vents or windward or a combination. The results showed that the opening configurations and wind speeds strongly affected the microclimate parameters and the ventilation. Also, there are different microclimate within each compartment due to the inside partition, which hinders air circulation between different parts of the greenhouse. [9]studied the effectiveness of ridge vent to wind-driven ventilation in a monoslope multi-span greenhouse. A three-dimensional LES simulation model and wind tunnel experiments were used. The numerical results were validated using the experimental results. In addition an analytical model was used to compute the ventilation rate. The study showed that the ventilation rates of the greenhouse with open ridge vents were much higher than that of greenhouse with closed ridge vents. Also, the windward ridge vent substantially increased the ventilation rate compared to leeward ridge vent. [10] studied the effect of increasing ventilation area on airflow patterns and thermal distribution in a traditional Colombian greenhouse using computational fluid dynamics. A passively ventilated greenhouse was considered and a numerical model was developed using two-dimensional CFD which was validated experimentally. The study showed that increase in roof ventilation areas reduced the averaged internal temperatures by up to 16%. The temperature homogeneity was improved and ventilation rate were increased by 19% with respect to the referenced scenario. In most of the above mentioned studies,the flows are two dimensional and steady. However, it is noticed that three dimensional transient mixed convection in a greenhouse with variable viscosity and thermal conductivity is not investigated widely. An adequate comprehension of mixed convection is essential to redesign ventilation systems of greenhouses. The objective of this paper is to investigate the velocity and heat transfer by considering the mixed convection,variable thermal conductivity and viscosity. The governing equations are solved by the finite volume method. The effect of various parameters on the velocity and temperature profiles determined.

2. Mathematical Model

We consider a three dimensional flow in a rectangular greenhouse with a horizontal roof, an inlet on the left wall and a fan on the right wall as shown in Fig. 1 below. The side walls and the upper wall are considered to be adiabatic while the bottom wall is isothermal. The no-slip condition is applied at the walls including the outlet where the fan is located. Further the fluid is unsteady with variable viscosity and thermal conductivity. The fluid viscosity is a function of temperature and is assumed to vary as an inverse function while the thermal conductivity is a linear function of temperature. The greenhouse is considered to be consisting of mature tomato crop. This study considers a turbulent mixed convection due to buoyancy forces and presence of the fan. The flow is governed by the time averaged mass, momentum and energy equations (1-5).

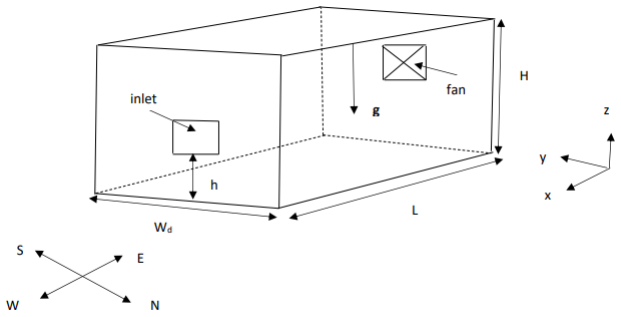

Fig. 1. Geometry of the problem

$$\frac{\partial \bar{u}}{\partial x}+\frac{\partial \bar{v}}{\partial y}+\frac{\partial \bar{w}}{\partial z}=0 \tag{1}$$

$$\begin{aligned}\rho\left[\frac{\partial \bar{u}}{\partial t}+\bar{u}\frac{\partial \bar{u}}{\partial x}+\bar{v}\frac{\partial \bar{u}}{\partial y}+\bar{w}\frac{\partial \bar{u}}{\partial z}\right]&=-\frac{\partial \bar{p}}{\partial x}+\frac{\partial}{\partial x}\left[\left(\frac{\mu_\infty}{1+\gamma\left(\bar{T}-T_\infty\right)}+\mu_t\right)\frac{\partial \bar{u}}{\partial x}\right]\\&+\frac{\partial}{\partial y}\left[\left(\frac{\mu_\infty}{1+\gamma\left(\bar{T}-T_\infty\right)}+\mu_t\right)\frac{\partial \bar{u}}{\partial y}\right]+\frac{\partial}{\partial z}\left[\left(\frac{\mu_\infty}{1+\gamma\left(\bar{T}-T_\infty\right)}+\mu_t\right)\frac{\partial \bar{u}}{\partial z}\right]\\&-I_{LAD}\rho C_d\bar{u}^2\end{aligned} \tag{2}$$

$$\begin{aligned}\rho\left[\frac{\partial \bar{v}}{\partial t}+\bar{u}\frac{\partial \bar{v}}{\partial x}+\bar{v}\frac{\partial \bar{v}}{\partial y}+\bar{w}\frac{\partial \bar{v}}{\partial z}\right]&=-\frac{\partial \bar{p}}{\partial y}+\frac{\partial}{\partial x}\left[\left(\frac{\mu_\infty}{1+\gamma\left(\bar{T}-T_\infty\right)}+\mu_t\right)\frac{\partial \bar{v}}{\partial x}\right]\\&+\frac{\partial}{\partial y}\left[\left(\frac{\mu_\infty}{1+\gamma\left(\bar{T}-T_\infty\right)}+\mu_t\right)\frac{\partial \bar{v}}{\partial y}\right]+\frac{\partial}{\partial z}\left[\left(\frac{\mu_\infty}{1+\gamma\left(\bar{T}-T_\infty\right)}+\mu_t\right)\frac{\partial \bar{v}}{\partial z}\right]\\&-I_{LAD}\rho C_d\bar{v}^2\end{aligned} \tag{3}$$

$$\begin{aligned}\rho\left[\frac{\partial \bar{w}}{\partial t}+\bar{u}\frac{\partial \bar{w}}{\partial x}+\bar{v}\frac{\partial \bar{w}}{\partial y}+\bar{w}\frac{\partial \bar{w}}{\partial z}\right]&=-\frac{\partial \bar{p}}{\partial z}+\frac{\partial}{\partial x}\left[\left(\frac{\mu_\infty}{1+\gamma\left(\bar{T}-T_\infty\right)}+\mu_t\right)\frac{\partial \bar{w}}{\partial x}\right]\\&+\frac{\partial}{\partial y}\left[\left(\frac{\mu_\infty}{1+\gamma\left(\bar{T}-T_\infty\right)}+\mu_t\right)\frac{\partial \bar{w}}{\partial y}\right]+\frac{\partial}{\partial z}\left[\left(\frac{\mu_\infty}{1+\gamma\left(\bar{T}-T_\infty\right)}+\mu_t\right)\frac{\partial \bar{w}}{\partial z}\right]\\&-I_{LAD}\rho C_d\bar{w}^2+\rho_\infty g\beta\left(\bar{T}-T_\infty\right)\end{aligned} \tag{4}$$

$$\begin{aligned}\rho c_p\left[\frac{\partial \bar{T}}{\partial t}+\bar{u}\frac{\partial \bar{T}}{\partial x}+\bar{v}\frac{\partial \bar{T}}{\partial y}+\bar{w}\frac{\partial \bar{T}}{\partial z}\right]&=\frac{\partial}{\partial x}\left[\kappa_\infty\left(1+c\left(\bar{T}-T_\infty\right)+\rho c_p\Gamma_t\right)\frac{\partial \bar{T}}{\partial x}\right]\\&+\frac{\partial}{\partial y}\left[\kappa_\infty\left(1+c\left(\bar{T}-T_\infty\right)+\rho c_p\Gamma_t\right)\frac{\partial \bar{T}}{\partial y}\right]+\frac{\partial}{\partial z}\left[\kappa_\infty\left(1+c\left(\bar{T}-T_\infty\right)+\rho c_p\Gamma_t\right)\frac{\partial \bar{T}}{\partial z}\right]\\&+\frac{I_{LA}\rho c_p\left(\bar{T}_w-\bar{T}\right)}{r_a}\end{aligned} \tag{5}$$

Where ρ is the density of air, $\overline{u},\overline{v}$ and $\overline{w}$ are the averaged velocity components in x,y,z-directions respectively, $\overline{p}$ is averaged pressure, μ_∞ is dynamical viscosity, μ_t is turbulent viscosity, I_{LAD} is the leaf area density index, C_d is the crop drag force coefficient, I_{LA} is crop stand leaf area index, r_a is the aerodynamic resistance,$\overline{T}$ is the averaged temperature, κ_∞ is the thermal conductivity, Γ_t is turbulent thermal conductivity, c_p is the specific heat at constant pressure, g is the gravitational force, γ is variable viscosity parameter, c is the variable thermal conductivity parameter and β is the thermal expansion coefficient. The terms $I_{LAD}\rho C_d\bar{u}^2$, $I_{LAD}\rho C_d\bar{v}^2$ and $I_{LAD}\rho C_d\bar{w}^2$ represents the tomato crop drag force in x,y and z directions while $\frac{I_{LA}\rho C_p\left(\bar{T}_w-\bar{T}\right)}{r_a}$[11] is transpiration sensible heat. The variable viscosity recommended by [12] is expressed as

$$\frac{1}{\mu}=\frac{1}{\mu_\infty}[1+\gamma(\overline{T}-T_\infty)] \tag{6}$$

Also the thermal conductivity is expressed as [13]

$$\kappa(T)=\kappa_\infty\left[1+c\left(\overline{T}-T_\infty\right)\right] \tag{7}$$

The two equations $k-\omega$ model [14] is used to close the URANS equations where

$$\mu_t = \frac{\rho k}{\omega} \tag{8}$$

and

$$\Gamma_t = \frac{\mu_t}{pr_t} \tag{9}$$

Where k is the turbulent kinetic energy, ω is the specific heat dissipation rate and pr_t is the turbulent Prandtl number.

3. Boundary Conditions

The boundary conditions for the above model are as follows:
for $t \le 0$:
$\overline{u} = \overline{v} = \overline{w} = \overline{T} = 0$
for $t > 0$:
At the walls we have:
$\overline{u} = \overline{v} = \overline{w} = 0$ at $x = 0$ and at $x = L$
$\overline{u} = \overline{v} = \overline{w} = 0$ at $y = 0$ and at $x = W_d$
$\overline{u} = \overline{v} = \overline{w} = 0$ at $z = 0$ and at $z = H$
$\overline{T} = T_w$ at the bottom wall
$\frac{\partial \overline{T}}{\partial n} = 0$ at the adiabatic walls
At the inlet
$\overline{u} = u_\infty$, $\overline{v} = \overline{w} = 0$, $\overline{T} = T_\infty$
At the oulet
$\overline{u} = u_f$, $\overline{v} = \overline{w} = 0$, $\frac{\partial \overline{T}}{\partial n} = 0$

4. Nondimensionalization

Nondimensionalization is the process of converting dimensional quantities to non-dimensional quantities. It ensures that the results are applicable to other geometrically similar configurations. In this study the following transformations are used to nondimensionalize the governing equations.

$$\begin{aligned} &x^\star = \frac{x}{L}, y^\star = \frac{y}{L}, z^\star = \frac{z}{L}, \bar{u}^\star = \frac{\bar{u}}{u_0}, \bar{v}^\star = \frac{\bar{v}}{u_0}, \bar{w}^\star = \frac{\bar{w}}{u_0}, t^\star = \frac{u_0}{L}t, \bar{p}^\star = \frac{\bar{p}}{\rho u_0^2}, \\ &\bar{T}^\star = \frac{\bar{T} - T_\infty}{\bar{T}_w - T_\infty}, \mu_t^\star = \frac{\mu_t}{\mu_\infty} \end{aligned} \tag{10}$$

Employing equation 10 into the governing equations (1- 5) and after dropping the stars results in;

$$\frac{\partial \bar{u}}{\partial x} + \frac{\partial \bar{v}}{\partial y} + \frac{\partial \bar{w}}{\partial z} = 0 \tag{11}$$

$$\begin{aligned} &\frac{\partial \bar{u}}{\partial t} + \bar{u}\frac{\partial \bar{u}}{\partial x} + \bar{v}\frac{\partial \bar{u}}{\partial y} + \bar{w}\frac{\partial \bar{u}}{\partial z} = -\frac{\partial \bar{p}}{\partial x} + \frac{\partial}{\partial x}\left[\left(\frac{1}{Re\left(1+a\bar{T}\right)} + \frac{\mu_t}{Re}\right)\frac{\partial \bar{u}}{\partial x}\right] \\ &+ \frac{\partial}{\partial y}\left[\left(\frac{1}{Re\left(1+a\bar{T}\right)} + \frac{\mu_t}{Re}\right)\frac{\partial \bar{u}}{\partial y}\right] + \frac{\partial}{\partial z}\left[\left(\frac{1}{Re\left(1+a\bar{T}\right)} + \frac{\mu_t}{Re}\right)\frac{\partial \bar{u}}{\partial z}\right] \\ &- I_{LAD}C_d L\bar{u}^2 \end{aligned} \tag{12}$$

$$\begin{aligned} &\frac{\partial \bar{v}}{\partial t} + \bar{u}\frac{\partial \bar{v}}{\partial x} + \bar{v}\frac{\partial \bar{v}}{\partial y} + \bar{w}\frac{\partial \bar{v}}{\partial z} = -\frac{\partial \bar{p}}{\partial y} + \frac{\partial}{\partial x}\left[\left(\frac{1}{Re\left(1+a\bar{T}\right)} + \frac{\mu_t}{Re}\right)\frac{\partial \bar{v}}{\partial x}\right] \\ &+ \frac{\partial}{\partial y}\left[\left(\frac{1}{Re\left(1+a\bar{T}\right)} + \frac{\mu_t}{Re}\right)\frac{\partial \bar{v}}{\partial y}\right] + \frac{\partial}{\partial z}\left[\left(\frac{1}{Re\left(1+a\bar{T}\right)} + \frac{\mu_t}{Re}\right)\frac{\partial \bar{v}}{\partial z}\right] \\ &- I_{LAD}C_d L\bar{v}^2 \end{aligned} \tag{13}$$

$$\frac{\partial \bar{w}}{\partial t}+\bar{u}\frac{\partial \bar{w}}{\partial x}+\bar{v}\frac{\partial \bar{w}}{\partial y}+\bar{w}\frac{\partial \bar{w}}{\partial z}=-\frac{\partial \bar{p}}{\partial z}+\frac{\partial}{\partial x}\left[\left(\frac{1}{Re\left(1+a\bar{T}\right)}+\frac{\mu_t}{Re}\right)\frac{\partial \bar{w}}{\partial x}\right]$$
$$+\frac{\partial}{\partial y}\left[\left(\frac{1}{Re\left(1+a\bar{T}\right)}+\frac{\mu_t}{Re}\right)\frac{\partial \bar{w}}{\partial y}\right]+\frac{\partial}{\partial z}\left[\left(\frac{1}{Re\left(1+a\bar{T}\right)}+\frac{\mu_t}{Re}\right)\frac{\partial \bar{w}}{\partial z}\right] \tag{14}$$
$$-I_{LAD}C_dL\bar{w}^2+\frac{Gr}{Re^2}\bar{T}$$

$$\frac{\partial \bar{T}}{\partial t}+\bar{u}\frac{\partial \bar{T}}{\partial x}+\bar{v}\frac{\partial \bar{T}}{\partial y}+\bar{w}\frac{\partial \bar{T}}{\partial z}=\frac{\partial}{\partial x}\left[\left(\frac{1+b\bar{T}}{PrRe}+\frac{\mu_t}{Pr_tRe}\right)\frac{\partial \bar{T}}{\partial x}\right]+\frac{\partial}{\partial y}\left[\left(\frac{1+b\bar{T}}{PrRe}+\frac{\mu_t}{Pr_tRe}\right)\frac{\partial \bar{T}}{\partial y}\right]$$
$$+\frac{\partial}{\partial z}\left[\left(\frac{1+b\bar{T}}{PrRe}+\frac{\mu_t}{Pr_tRe}\right)\frac{\partial \bar{T}}{\partial z}\right]+\frac{I_{LA}L\left(1-\bar{T}\right)}{u_0r_a} \tag{15}$$

The boundary conditions in non-dimensional form are given by:
for $t \leq= 0$:
$\overline{u}=\overline{v}=\overline{w}=\overline{T}=0$
for $t>0$:
At the walls we have:
$\overline{u}=\overline{v}=\overline{w}=0$ at $x=0$ and at $x=L$
$\overline{u}=\overline{v}=\overline{w}=0$ at $y=0$ and at $x=W_d$
$\overline{u}=\overline{v}=\overline{w}=0$ at $z=0$ and at $z=H$
$\overline{T}=1$ at the bottom wall
$\frac{\partial \overline{T}}{\partial n}=0$ at the adiabatic walls
At the inlet
$\overline{u}=1$, $\overline{v}=\overline{w}=0$, $\overline{T}=0$
At the oulet
$\overline{u}=u_f$, $\overline{v}=\overline{w}=0$, $\frac{\partial \overline{T}}{\partial n}=0$
The non-dimensional numbers obtained are; $Re=\frac{\rho u_0 L}{\mu_\infty}$ is the Reynolds' number, $Ri=\frac{Gr}{Re^2}$ is the Richardson number,$Gr=\frac{g\beta L^3(\bar{T}_w-T_\infty)}{u_0^2}$ is the Grashof number, $Pr=\frac{\mu_\infty c_p}{k_\infty}$ is the prandtl number. The variable viscosity parameter is $\gamma<0$ and $a=\gamma(\bar{T}_w-T_\infty)$. $c>0$ represent the variable thermal conductivity parameter and $b=c(T-T_\infty)$

5. Numerical Technique

The non-dimensional governing equations(11- 15) are solved numerically by finite volume method [15]. First the domain is divided into a number of finite sized sub-domains(Control volumes). Then the governing partial differential equations are disretized by integrating over each subdomain. The gradients (and hence fluxes) at the volume faces are linearly approximated. The resulting system of linear algebraic equations is solved to obtain the distribution properties at the nodal points. TriDiagonal Matrix Algorithm(TDMA),also known as Thomas algorithm is used to solve the system of algebraic equations with a tridiagonal coefficient matrix. The control volume has a centre node P surrounded by six other nodes identified as east, west, north, south, top and bottom with the notations E, W, N,S,T and B respectively. The cell faces have the notations e, w, n, s, t and b referring to east, west, north, south, top and bottom faces respectively. The distances between the nodes W and P, P and E, S and P, P and N, B and P and P and T are denoted by δx_{WP}, δx_{PE}, δy_{SP}, δy_{PN}, δz_{BP} and δz_{PT} respectively. The distances between the east and west, north and south and top and bottom faces are respectively Δx, Δy and Δz. The governing equations are discritized as follows:
The x-direction momentum equation 12 (and all other equations) is first integrated over the control volume and then with respect to time as follows;

$$\int_t^{t+\Delta t}\int_{Cv}\frac{\partial \bar{u}}{\partial t}dvdt+\int_t^{t+\Delta t}\int_{Cv}\frac{\partial(\bar{u}\bar{u})}{\partial x}dvdt+\int_t^{t+\Delta t}\int_{Cv}\frac{\partial(\bar{u}\bar{v})}{\partial y}dvdt+\int_t^{t+\Delta t}\int_{Cv}\frac{\partial(\bar{u}\bar{w})}{\partial z}dvdt$$
$$=\int_t^{t+\Delta t}\int_{Cv}-\frac{\partial \bar{p}}{\partial x}dvdt+\int_t^{t+\Delta t}\int_{Cv}\frac{\partial}{\partial x}\left[N\frac{\partial \bar{u}}{\partial x}\right]dvdt+\int_t^{t+\Delta t}\int_{Cv}\frac{\partial}{\partial y}\left[N\frac{\partial \bar{u}}{\partial y}\right]dvdt \tag{16}$$
$$+\int_t^{t+\Delta t}\int_{Cv}\frac{\partial}{\partial z}\left[\frac{\partial \bar{u}}{\partial z}\right]dvdt-\int_t^{t+\Delta t}\int_{Cv}Ddvdt$$

where $N=\frac{1}{Re(1+a\bar{T})}+\frac{\mu_t}{Re}$ and $D=I_{LAD}c_dLu^2$
Applying the Gauss' divergence theorem[16] to the convective and diffusive terms and changing the order of integra-

tion in the rate of change term, equation 16 can be written as

$$\begin{aligned}&\int_{Cv}\left[\int_t^{t+\Delta t}\frac{\partial \bar{u}}{\partial t}dt\right]dv+\int_t^{t+\Delta t}\left[\int_s n\cdot(\bar{u}\bar{u})\,dA\right]dt+\int_t^{t+\Delta t}\left[\int_s n\cdot(\bar{u}\bar{v})\,dA\right]dt+\int_t^{t+\Delta t}\left[\int_s n\cdot(\bar{u}\bar{w})\,dA\right]dt\\&=\int_t^{t+\Delta t}\int_{Cv}-\frac{\partial \bar{p}}{\partial x}dvdt+\int_t^{t+\Delta t}\left[\int_s n\cdot\left(N\frac{\partial u}{\partial x}\right)dA\right]dt+\int_t^{t+\Delta t}\left[\int_s n\cdot\left(N\frac{\partial u}{\partial y}\right)dA\right]dt\\&+\int_t^{t+\Delta t}\left[\int_s n\cdot\left(N\frac{\partial u}{\partial z}\right)dA\right]dt-\int_t^{t+\Delta t}\int_{Cv}Ddvdt\end{aligned}\tag{17}$$

For the first term on the left hand side, if the velocity at a node is assumed to prevail over the control volume,then:

$$\int_{Cv}\left[\int_t^{t+\Delta t}\frac{\partial \bar{u}}{\partial t}dt\right]dv=\left(\bar{u}_p-\bar{u}_p^0\right)\Delta v\tag{18}$$

Where superscript '0' refers to velocities at time t while velocities at $t+\Delta t$ are not superscripted. Also, intergating the the convective terms results in

$$\begin{aligned}&\int_t^{t+\Delta t}\int_s n\cdot(\bar{u}\bar{u})\,dAdt+\int_t^{t+\Delta t}\int_s n\cdot(\bar{u}\bar{v})\,dAdt+\int_t^{t+\Delta t}\int_s n\cdot(\bar{u}\bar{w})\,dAdt\\&=\int_t^{t+\Delta t}\left[(\bar{u}\bar{u})_e\Delta x\Delta z-(\bar{u}\bar{u})_w\Delta x\Delta z\right]dt+\int_t^{t+\Delta t}\left[(\bar{u}\bar{v})_n\Delta y\Delta z-(\bar{u}\bar{v})_s\Delta y\Delta z\right]dt\\&+\int_t^{t+\Delta t}\left[(\bar{u}\bar{w})_t\Delta x\Delta y-(\bar{u}\bar{w})_b\Delta x\Delta y\right]dt\end{aligned}\tag{19}$$

Employing fully implicit scheme[15] equation 19 becomes

$$\begin{aligned}&\int_t^{t+\Delta t}\int_s n\cdot(\bar{u}\bar{u})\,dAdt+\int_t^{t+\Delta t}\int_s n\cdot(\bar{u}\bar{v})\,dAdt+\int_t^{t+\Delta t}\int_s n\cdot(\bar{u}\bar{w})\,dAdt=\left[\bar{u}_e\left(\frac{\bar{u}_P+\bar{u}_E}{2}\right)\Delta x\Delta z\Delta t\right]\\&-\left[\bar{u}_w\left(\frac{\bar{u}_W+\bar{u}_P}{2}\right)\Delta x\Delta z\Delta t\right]+\left[\bar{v}_n\left(\frac{\bar{u}_P+\bar{u}_N}{2}\right)\Delta y\Delta z\Delta t\right]-\left[\bar{v}_s\left(\frac{\bar{u}_S+\bar{u}_P}{2}\right)\Delta y\Delta z\Delta t\right]\\&+\left[\bar{w}_t\left(\frac{\bar{u}_P+\bar{u}_T}{2}\right)\Delta x\Delta y\Delta t\right]+\left[\bar{w}_b\left(\frac{\bar{u}_B+\bar{u}_P}{2}\right)\Delta x\Delta y\Delta t\right]\end{aligned}\tag{20}$$

Applying central differencing and employing fully implicit scheme the diffusive terms can be written as:

$$\begin{aligned}&\int_t^{t+\Delta t}\left[\int_s n\cdot\left(N\frac{\partial u}{\partial x}\right)dA\right]dt+\int_t^{t+\Delta t}\left[\int_s n\cdot(N\frac{\partial u}{\partial y})dA\right]dt+\int_t^{t+\Delta t}\left[\int_s n\cdot(N\frac{\partial u}{\partial z})dA\right]dt\\&=\left[N_e\left(\frac{\bar{u}_E-\bar{u}_P}{\delta x_{PE}}\right)\Delta x\Delta z\Delta t-N_w\left(\frac{\bar{u}_P-\bar{u}_W}{\delta x_{WP}}\right)\Delta x\Delta z\Delta t\right]+\left[N_n\left(\frac{\bar{u}_N-\bar{u}_P}{\delta y_{PN}}\right)\Delta y\Delta z\Delta t-N_s\left(\frac{\bar{u}_P-\bar{u}_S}{\delta y_{SP}}\right)\Delta y\Delta z\Delta t\right]\\&+\left[N_t\left(\frac{\bar{u}_T-\bar{u}_P}{\delta z_{PT}}\right)\Delta x\Delta y\Delta t-N_b\left(\frac{u_P-u_B}{\delta z_{BP}}\right)\Delta x\Delta y\Delta t\right]\end{aligned}\tag{21}$$

Expanding the source term $D=-I_{LAD}C_dLu^2$, using the Taylor's series [17] yields

$$D(u_P)=D\left(u_P^0\right)+\left(\frac{\partial D}{\partial u_P}\right)^0\left(u_P-u_P^0\right)=\left(\frac{\partial D}{\partial u_P}\right)^0u_P+D\left(u_P^0\right)-\left(\frac{\partial D}{\partial u_P}\right)^0u_P^0\tag{22}$$

Therefore

$$D(u_P)=-2I_{LAD}C_dLu_P^0u_P-I_{LAD}C_dL(u_P^0)^2+2I_{LAD}C_dL(u_P^0)^2=-2I_{LAD}C_dLu_P^0u_P+I_{LAD}C_dL(u_P^0)^2$$

Letting

$$fluxC_c=-2I_{LAD}C_dLu_P^0u_P\Delta v\tag{23}$$

$$fluxV_c=I_{LAD}C_dL(u_P^0)^2\Delta v\tag{24}$$

Where $fluxC_c$ is the implicit part and $fluxV_c$ is the explicit part, integrating equations 23 and equation 24 with respect to time yield;

$$\int_t^{t+\Delta t}[-2I_{LAD}C_dLu_P^0u_P\Delta v]dt=-2I_{LAD}C_dLu_P^0u_P\Delta v\Delta t\tag{25}$$

and

$$\int_t^{t+\Delta t} [I_{LAD} C_d L (u_P^0)^2 \Delta v] dt = I_{LAD} C_d L (u_P^0)^2 \Delta v \Delta t \tag{26}$$

For the pressure terms, the volume integral is transformed into surface integral i.e

$$\int_{Cv} \frac{\partial p}{\partial x} dv = \int_s p dy dz \tag{27}$$

Rewriting the surface integral as a summation of fluxes over the faces the above equation becomes

$$\int_{Cv} \frac{\partial p}{\partial x} dv = \int_s p dy dz = p_e \Delta y \Delta z - p_w \Delta y \Delta z = (p_e - p_w) \Delta y \Delta z = (p_e - p_w) \frac{\Delta v}{\Delta x} \tag{28}$$

applying linear interpolation[15] to the above equation yields

$$\begin{aligned} &\int_{Cv} \frac{\partial p}{\partial x} dv = \int_s p dy dz = p_e \Delta y \Delta z - p_w \Delta y \Delta z = (p_e - p_w) \Delta y \Delta z = (p_e - p_w) \frac{\Delta v}{\Delta x} \\ &= \left[\frac{1}{2} (P_E + P_P) - \frac{1}{2} (P_P + P_W) \right] \frac{\Delta v}{\Delta x} = \frac{P_E - P_W}{2\Delta x} \Delta v \end{aligned} \tag{29}$$

integrating with respect to time gives

$$\int_t^{t+\Delta t} \int_{Cv} \frac{\partial p}{\partial x} dv = \int_t^{t+\Delta t} \frac{P_E - P_W}{2\Delta x} \Delta v = \frac{P_E - P_W}{2\Delta x} \Delta v \Delta t \tag{30}$$

Combining all discretized terms, the x-direction equation in discretized form is

$$\begin{aligned} &(u_P - u_P^0) \Delta x \Delta y \Delta z + u_e \left(\frac{u_P + u_E}{2} \right) \Delta x \Delta z \Delta t - u_w \left(\frac{u_W + u_P}{2} \right) \Delta x \Delta z \Delta t + v_n \left(\frac{u_P + u_N}{2} \right) \Delta y \Delta z \Delta t \\ &- v_s \left(\frac{u_S + u_P}{2} \right) \Delta y \Delta z \Delta t + w_t \left(\frac{u_P + u_T}{2} \right) \Delta x \Delta y \Delta t - w_b \left(\frac{u_B + u_P}{2} \right) \Delta x \Delta y \Delta t = N_e \left(\frac{u_E - u_P}{\delta x_{PE}} \right) \Delta x \Delta z \Delta t \\ &- N_w \left(\frac{u_P - u_W}{\delta x_{WP}} \right) \Delta x \Delta z \Delta t + N_n \left(\frac{u_N - u_P}{\delta y_{PN}} \right) \Delta y \Delta z \Delta t - N_s \left(\frac{u_P - u_S}{\delta y_{SP}} \right) \Delta y \Delta z \Delta t + N_t \left(\frac{u_T - u_P}{\delta z_{PT}} \right) \Delta y \Delta y \Delta t \\ &- N_b \left(\frac{u_P - u_B}{\delta z_{BP}} \right) \Delta x \Delta y \Delta t + \left(\frac{p_E - p_W}{2\Delta x} \right) \Delta x \Delta y \Delta z \Delta t - \left(2 I_{LAD} C_d L u_P^0 u_P \right) \Delta x \Delta y \Delta z \Delta t \\ &+ I_{LAD} C_d L \left(u_P^0 \right)^2 \Delta x \Delta y \Delta z \Delta t \end{aligned} \tag{31}$$

Since$\Delta x = \Delta y = \Delta z$, dividing equation 31 by surface area and Δt and putting the like terms together yields

$$\begin{aligned} &[\frac{\Delta x}{\Delta t} + (\frac{N_e}{\delta x_{PE}} - \frac{u_e}{2}) + (\frac{N_w}{\delta x_{WP}} + \frac{u_w}{2}) + (\frac{N_n}{\delta y_{PN}} - \frac{v_n}{2}) + (\frac{N_s}{\delta y_{SP}} + \frac{v_s}{2}) + (\frac{N_t}{\delta z_{PT}} - \frac{w_t}{2}) \\ &+ (\frac{N_b}{\delta z_{BP}} + \frac{w_b}{2}) + (u_e - u_w + v_n - v_s + w_t - w_b) + 2 I_{LAD} C_d L \Delta x u_P^0] u_P = (\frac{N_e}{\delta x_{PE}} - \frac{u_e}{2}) u_E \\ &+ (\frac{N_w}{\delta x_{WP}} + \frac{u_w}{2}) u_W + (\frac{N_n}{\delta y_{SP}} - \frac{v_n}{2}) u_N + (\frac{N_s}{\delta y_{SP}} + \frac{v_s}{2}) u_S + (\frac{N_t}{\delta z_{PT}} - \frac{w_t}{2}) u_T + (\frac{N_b}{\delta z_{BP}} + \frac{w_b}{2}) u_B \\ &+ \frac{\Delta x}{\Delta t} u_P^0 + \frac{p_E}{2} - \frac{p_W}{2} + I_{LAD} C_d L \Delta x u_P^0 \end{aligned} \tag{32}$$

Equation 32 can be written as

$$a_P u_p = a_E u_E + a_W u_W + a_N u_N + a_S u_S + a_T u_T + a_B u_B + a_P^0 u_P^0 + S_u + \Delta p \tag{33}$$

Where $a_P = a_P^0 + a_E + a_W + a_N + a_S + a_T + a_B - S_P$, $a_P^0 = \frac{\Delta x}{\Delta t}$, $a_E = \left(\frac{N_e}{\delta x_{PE}} - \frac{u_e}{2} \right)$, $a_W = \left(\frac{N_w}{\delta x_{WP}} + \frac{u_w}{2} \right)$, $a_N = \left(\frac{N_n}{\delta y_{PN}} - \frac{v_n}{2} \right)$, $a_S = \left(\frac{N_s}{\delta y_{SP}} + \frac{v_s}{2} \right)$, $a_T = \left(\frac{N_t}{\delta z_{PT}} - \frac{w_t}{2} \right)$, $a_B = \left(\frac{N_b}{\delta z_{BP}} + \frac{w_b}{2} \right)$, $S_P = -2 I_{LAD} C_d L \Delta x u_P^0$,
$S_u = I_{LAD} C_d L \Delta x u_P^0$, $\Delta p = \frac{p_E}{2} - \frac{p_W}{2}$
Similarly the discretized y-direction equation is

$$a_P v_p = a_E v_E + a_W v_W + a_N v_N + a_S v_S + a_T v_T + a_B v_B + a_P^0 v_P^0 + S_u + \Delta p \tag{34}$$

Where
$a_P = a_P^0 + a_E + a_W + a_N + a_S + a_T + a_B - S_P$, $a_P^0 = \frac{\Delta y}{\Delta t}$, $a_E = \left(\frac{N_e}{\delta x_{PE}} - \frac{u_e}{2} \right)$, $a_W = \left(\frac{N_w}{\delta x_{WP}} + \frac{u_w}{2} \right)$,
$a_N = \left(\frac{N_n}{\delta y_{PN}} - \frac{v_n}{2} \right)$, $a_S = \left(\frac{N_s}{\delta y_{SP}} + \frac{v_s}{2} \right)$, $a_T = \left(\frac{N_t}{\delta z_{PT}} - \frac{w_t}{2} \right)$, $a_B = \left(\frac{N_b}{\delta z_{BP}} + \frac{w_b}{2} \right)$, $S_P = -2 I_{LAD} C_d L \Delta y v_P^0$,

$S_u = I_{LAD} C_d L \Delta y v_P^0$, $\Delta p = \frac{p_N}{2} - \frac{p_S}{2}$,
In a similar way the discretized z-direction momentum equation is

$$a_P w_p = a_E w_E + a_W w_W + a_N w_N + a_S w_S + a_T w_T + a_B w_B + a_P^0 w_P^0 + S_u + \Delta p + Ri T_P^0 \tag{35}$$

Where
$a_P = a_P^0 + a_E + a_W + a_N + a_S + a_T + a_B - S_P$, $a_P^0 = \frac{\Delta z}{\Delta t}$, $a_E = \left(\frac{N_e}{\delta x_{PE}} - \frac{u_e}{2}\right)$, $a_W = \left(\frac{N_w}{\delta x_{WP}} + \frac{u_w}{2}\right)$,
$a_N = \left(\frac{N_n}{\delta y_{PN}} - \frac{v_n}{2}\right)$, $a_S = \left(\frac{N_s}{\delta y_{SP}} + \frac{v_s}{2}\right)$, $a_T = \left(\frac{N_t}{\delta z_{PT}} - \frac{w_t}{2}\right)$, $a_B = \left(\frac{N_b}{\delta z_{BP}} + \frac{w_b}{2}\right)$, $S_P = -2 I_{LAD} C_d L \Delta z w_P^0$
$S_u = I_{LAD} C_d L \Delta z w_P^0$, $\Delta p = \frac{p_T}{2} - \frac{p_B}{2}$

The energy equation is also discretized as

$$a_P T_p = a_E T_E + a_W T_W + a_N T_N + a_S T_S + a_T T_T + a_B T_B + a_P^0 T_P^0 + S_u \tag{36}$$

Where $a_P = a_P^0 + a_E + a_W + a_N + a_S + a_T + a_B - S_P$, $a_P^0 = \frac{\Delta x}{\Delta t}$, $a_E = \left(\frac{M_e}{\delta x_{PE}} - \frac{u_e}{2}\right)$, $a_W = \left(\frac{M_w}{\delta x_{WP}} + \frac{u_w}{2}\right)$,
$a_N = \left(\frac{M_n}{\delta y_{PN}} - \frac{v_n}{2}\right)$, $a_S = \left(\frac{M_s}{\delta y_{SP}} + \frac{v_s}{2}\right)$, $a_T = \left(\frac{M_t}{\delta z_{PT}} - \frac{w_t}{2}\right)$, $a_B = \left(\frac{M_b}{\delta z_{BP}} + \frac{w_b}{2}\right)$,
$S_P = \frac{I_{LA} L}{u_0 r_a} \Delta z$, $S_u = \frac{\Delta x}{\Delta t} T_P^0$, $\frac{I_{LA} L}{u_0 r_a} \Delta z$

6. Results and Discussions

Numerical computations are performed and the effects of flow parameters on the fluid flow within a three-dimensional greenhouse are presented graphically and discussed. The results are analyzed in terms of velocity and temperature profiles over a wide range of Reynolds number ($10,000 \leq Re \leq 14,000$), Richardson number ($0.01 \leq Ri \leq 10$) and the aspect ratio ($1 \leq AR \leq 2$).The working fluid is air with Prandtl number $Pr = 0.71$ and the aspect ratio $AR = \frac{H}{L}$. The effects of Reynolds number, Richardson number, Prandtl number and aspect ratio on the velocity and temperature profiles are shown in figures (2-13).

Velocity and Temperature profiles

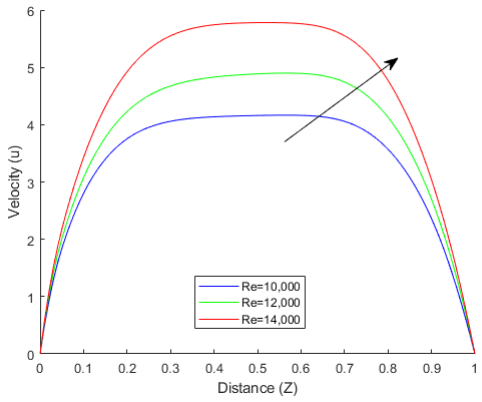

Fig. 2. The velocity profiles for various values of Re at X=0.5,Y=0.5 with Pr=0.71,AR=1 and Ri=0.1

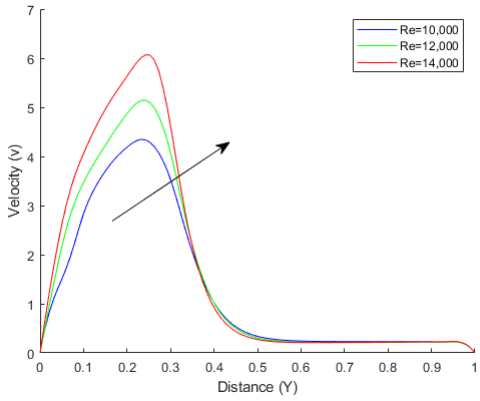

Fig. 3. The velocity profiles for various values of Re at X=0.5,Z=0.5 with Pr=0.71,AR=1 and Ri=0.1

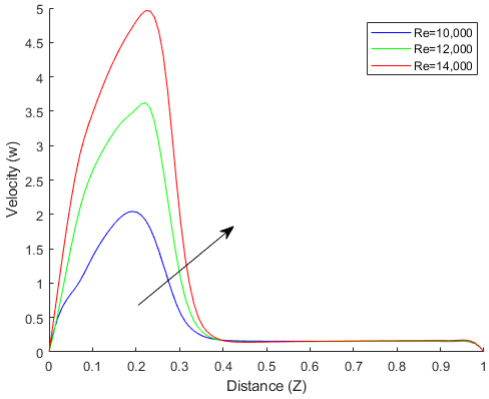

Fig. 4. The velocity profiles for various values of Re at X=0.5,Y=0.5 with Pr=0.71,AR=1 and Ri=0.1

Figures(2-4) show the influence of Reynolds number on the velocity profiles of the fluid holding Pr, AR and Ri as constants. The Reynolds number represent the ratio of inertia forces to viscous forces. It is observed that an increase in Reynolds number leads to an increase in velocity profiles of the fluid. Increasing the Reynolds number signifies a decrease in the viscous forces and thus the inertia forces dominates the flow. As a result, the velocity profiles increase due to the decrease of the viscous forces since the boundary layer does not extend much into the flow region as is the case when viscous forces dominate the flow. Figures(5-7) show the influence of Richardson number on the velocity profiles of the fluid holding Re, AR and Pr as constants. It is observed that an increase in Richardson number leads to an increase in velocity profiles of the fluid.This is due to the fact that the buoyancy forces become predominant hence

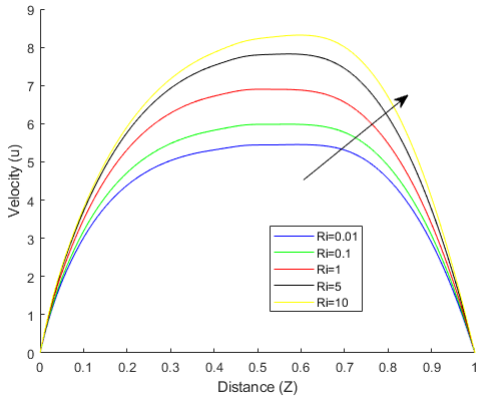

Fig. 5. The velocity profiles for various values of Ri at X=0.5,Y=0.5 with Pr=0.71,AR=1 and Re=10,000

the velocity profiles increase. Figures 8 and 9 show the influence of aspect ratio to the velocity profiles. It is observed that an increase in the aspect ratio results in increase in the velocity profiles. This is attributed by the fact that the strength of the viscous effects relative to the buoyancy forces decrease with increasing aspect ratio. Figure 10 shows the influence of Reynolds number on the temperature profiles. It is observed that as the Reynolds number increase, the temperature profiles decrease. In gases viscosity arises from molecules traversing the layers of flow and transferring momentum between the layers which can be thought as the frictional force between the layers. As the thermal agitation of the molecules is increased the viscosity increases and hence viscosity increases with temperature. Thus as the Reynolds number increase, the temperature decrease since the inertia forces dominate the flow. Figure 11 shows the influence of prandtl number on the temperature profiles. It is observed that as the Prandtl number increase the

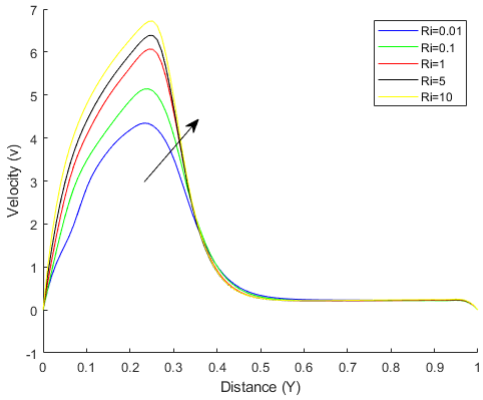

Fig. 6. The velocity profiles for various values of Ri at X=0.5,Z=0.5 with Pr=0.71,AR=1 and Re=10,000

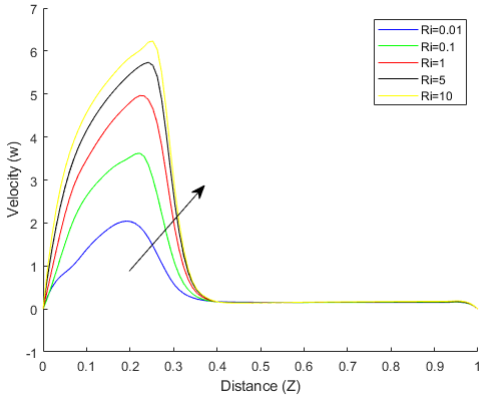

Fig. 7. The velocity profiles for various values of Ri at X=0.5,Y=0.5 with Pr=0.71,AR=1 and Re=10,000

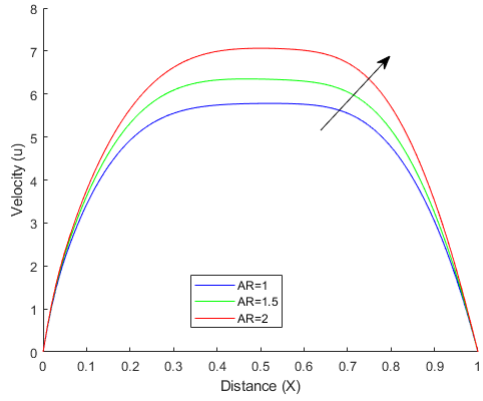

Fig. 8. The velocity profiles for various values of AR at Y=0.5,Z=0.5 with Pr=0.71,Ri=0.1 and Re=10,000

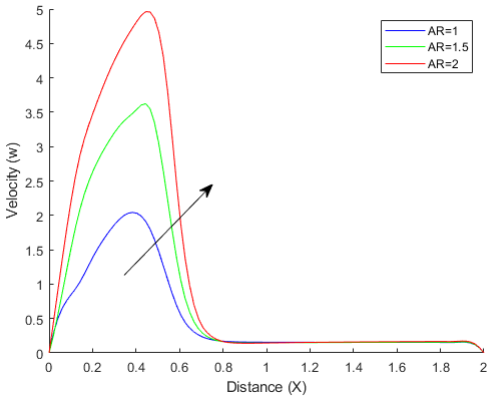

Fig. 9. The velocity profiles for various values of AR at Y=0.5,Z=0.5 with Pr=0.71, Ri=0.1 and Re=10,000

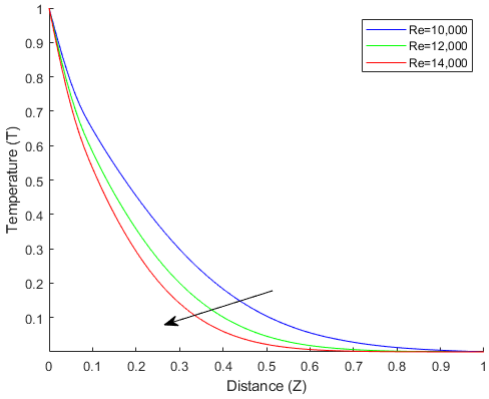

Fig. 10. The Temperature profiles for various values of Re at X=0.5,Y=0.5 with Pr=0.71, Ri=0.1 and AR=1

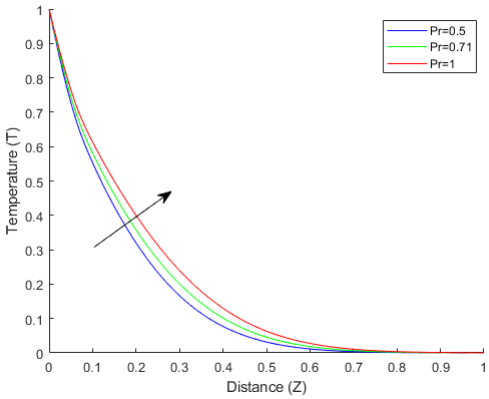

Fig. 11. The Temperature profiles for various values of Pr at X=0.5,Y=0.5 with Re=10,000, Ri=0.1 and AR=1

temperature profiles increase. Prandtl number gives the ratio of momentum diffusivity to thermal diffusivity. At high Prandtl number the momentum diffusivity dominate while at low Prandtl number the thermal diffusivity is dominant. An increase in Prandtl number indicate decrease in thermal diffusivity leading to an increase in internal temperature of the fluid. Figure 12 shows the influence of Richardson number on the temperature profiles. It is observed that as the Richardson number increase the temperature profiles decrease. Increasing the Richardson number reduces the thermal boundary layer thickness hence the decrease in temperature. Figure 13 shows the influence of aspect ratio on the temperature profiles. It is observed that as the aspect ratio increase the temperature profiles increase. Increasing the aspect ratio leads to an increase the thermal inertia hence the increase in greenhouse temperature.

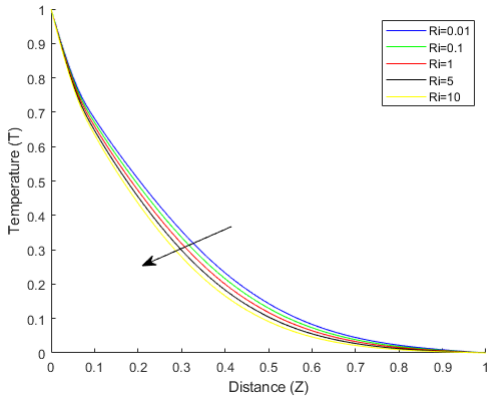

Fig. 12. The Temperature profiles for various values of Ri at X=0.5,Y=0.5 with Re=10,000, pr=0.71 and AR=1

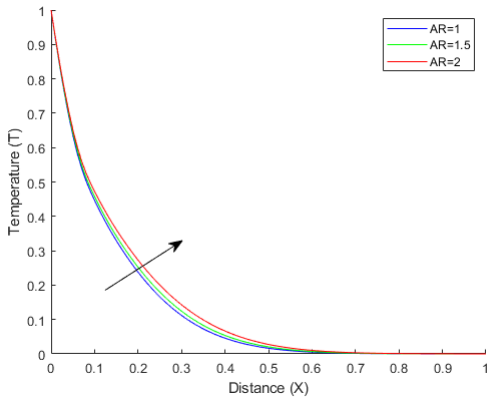

Fig. 13. The Temperature profiles for various values of AR at Y=0.5,Z=0.5 with Re=10,000, Pr=0.71 and Ri=0.1

7. Conclusion

Three dimensional turbulent mixed convection of heat in a greenhouse with horizontal roof is analyzed in this study. The analysis is carried out taking into consideration the crop effect i.e. crop drag force and sensible heat released during transpiration. The effect of various parameters are determined and observations are summarized as follows:

1 Velocity components are increasing functions of Reynolds number. However the temperature decrease with an increase in Reynolds number.

2 Velocity components are increasing functions of Richardson number. However the temperature decrease with an increase in Richardson number Ri.

3 An increase in aspect ratio AR leads to a increase in both the velocity and temperature profiles.

4 Increasing the greenhouse length decreases the internal temperature.

Acknowledgements

The author(s) highly appreciate the Pan African University, Institute for Basic Sciences, Technology, and Innovation for funding and support of this research project.

References

[1] G. Giacomelli and W. Roberts, Tech. Rep., D-03130-17-92 (1983).
[2] G. P. Bot, Ph.D. thesis, Bot (1983).
[3] K. Popovski, GHC Bulletin (1997).
[4] S. Wang and T. Boulard, Journal of agricultural engineering research **75**, 27 (2000).
[5] J. Roy and T. Boulard, in *International Conference on Sustainable Greenhouse Systems-Greensys2004 691* (2004), pp. 457–464.
[6] H. Moriyama, C. Kubota, K. Kurata, M. Hayashi, N. Sabeh, P. Romero, G. A. Giacomelli, S. Sase, and M. Ishii, in *International Symposium on Greenhouse Cooling 719* (2006), pp. 385–392.
[7] E. Rico-Garcia, J. Reyes-Araiza, and G. Herrera-Ruiz, in *International Symposium on Greenhouse Cooling 719* (2006), pp. 325–332.
[8] S. O. Khaoua, P. Bournet, C. Migeon, T. Boulard, and G. Chasseriaux, Biosystems Engineering **95**, 83 (2006).
[9] C.-R. Chu and T.-W. Lan, Biosystems Engineering **186**, 279 (2019).
[10] E. A. Villagran Munar and C. R. Bojacá Aldana (2020).
[11] H. Fatnassi, T. Boulard, C. Poncet, and M. Chave, Biosystems Engineering **93**, 301 (2006).
[12] F. Lai and F. Kulacki, International Journal of Heat and Mass Transfer **33**, 1028 (1990).
[13] J. C. Slattery, Chemical Engineering Education **6**, 174 (1972).
[14] D. C. Wilcox et al., *Turbulence modeling for CFD*, vol. 2 (DCW industries La Canada, CA, 1998).
[15] H. K. Versteeg and W. Malalasekera, *An introduction to computational fluid dynamics: the finite volume method* (Pearson education, 2007).
[16] H. J. Weber and G. B. Arfken, *Essential mathematical methods for physicists, ISE* (Elsevier, 2003).
[17] E. W. Weisstein, https://mathworld. wolfram. com/ (2004).